Inorg. Chem. **2007**, *46*, 8722–8727

$Ca_4Au_{10}In_3$: Synthesis, Structure, and Bonding Analysis. The Chemical and Electronic Transformations from the Isotypic Zr_7Ni_{10} Intermetallic

Qisheng Lin and John D. Corbett*

Department of Chemistry, Iowa State University, Ames, Iowa 50010

Received May 22, 2007

The title compound, $Ca_4Au_{10}In_3$ (e/a = 1.59), was synthesized by conventional high-temperature solid-state reactions and structurally analyzed by single-crystal X-ray diffraction: space group *Cmca*, $a = 13.729(4)$ Å, $b = 10.050(3)$ Å, $c = 10.160(3)$ Å, $Z = 4$. The structure, isotypic with that of Zr_7Ni_{10}, features a novel three-dimensional $[Au_{10}In_3]$ polyanionic framework built from sinusoidal Au layers that are interconnected by significant Au–Au and Au–In interactions. A prominent electronic feature is the presence of a pseudogap and empty bonding states above the Fermi level according to LMTO calculations, reminiscent of the tunable electronic properties discovered for Mg_2Zn_{11}-type phases. The natures of the chemical and electronic redistributions from Zr_7Ni_{10} to $Ca_4Au_{10}In_3$ are considered. The Au backbone appears to be particularly important.

Introduction

Recent explorations of polar intermetallic phases have mainly focused on the introduction of late transition metals into classic Zintl phases or their neighbors,[1−5] through which lower valence electron counts per atom (e/a) are achieved. Studies of these new phases, which electronically approach Hume−Rothery phases, have greatly improved our understanding of the interplay among composition, structure, bonding, and properties of such compounds.

One important facet in this area that has caught our attention[6−10] is the opportunity to explore the intermetallic regions populated by quasicrystals (QCs) and their approximant crystals (ACs),[11] which are fairly new for solid-state chemists. The structures of ACs apparently always feature condensed multiple-shell clusters with pseudo-5-fold symmetry, i.e., in the Mackay-,[12] Bergman-,[13] and Tsai-type[14] examples, with low e/a values around 2.0. Thus, these electron-poorer phases in general do not obey the Zintl[15] or Wade−Mingos rules[16] applicable to networks or clusters that exhibit more localized bonding. Rather, they are perhaps better regarded as relatives of Hume−Rothery phases.[17−19] Recently, we have discovered a route by which AC and QC examples may be achieved synthetically starting with promising intermetallic structures such as those of the isotypic $Mg_2Cu_6Ga_5$,[6] Mg_2Zn_{11},[20] and $Na_2Au_6In_5$[21] family. The success of the procedures may be ascribed to their special structural and bonding features (mini Bergman clusters, etc.) and to the presence of a pseudogap and empty bonding states near their Fermi levels to which one can tune by suitable chemical substitutions.

In this article, we describe the discovery of $Ca_4Au_{10}In_3$, a novel phase showing an unprecedented 3D Au−In polyanionic framework. This has a notably lower e/a value, 1.59,

* To whom correspondence should be addressed. E-mail: jcorbett@iastate.edu.

(1) Corbett, J. D. In *Chemistry, Structure, and Bonding of Zintl Phases and Ions*; Kauzlarich, S. M., Ed.; VCH: New York, 1996; p 139.
(2) Corbett, J. D. *Angew. Chem., Int. Ed.* **2000**, *39*, 670.
(3) Dong, Z.-C.; Corbett, J. D. *Angew. Chem., Int. Ed. Engl.* **1996**, *35*, 1006.
(4) Miller, G. J.; Lee, C.-S.; Choe, W. In *Inorganic Chemistry Highlights*; Meyer, G., Naumann, D., Wesemann, L., Eds.; Wiley-VCH: Weinheim, Germany, 2002; pp 21−53.
(5) Nordell, K. J.; Miller, G. J. *Inorg. Chem.* **1999**, *38*, 579.
(6) Lin, Q.; Corbett, J. D. *Inorg. Chem.* **2003**, *42*, 8762.
(7) Lin, Q.; Corbett, J. D. *Inorg. Chem.* **2004**, *43*, 1912.
(8) Lin, Q.; Corbett, J. D. *Inorg. Chem.* **2005**, *44*, 512.
(9) Lin, Q.; Corbett, J. D. *J. Am. Chem. Soc.* **2005**, *127*, 12786.
(10) Lin, Q.; Corbett, J. D. *J. Am. Chem. Soc.* **2006**, *128*, 13268.
(11) Janot, C. *Quasicrystals: A Primer*, 2nd ed.; Oxford University Press: Oxford, U.K., 1994.
(12) Mackay, A. L. *Acta Crystallogr.* **1962**, *15*, 916.
(13) Bergman, G.; Waugh, J. L. T.; Pauling, L. *Acta Crystallogr.* **1957**, *10*, 254.
(14) Tsai, A. P.; Guo, J. Q.; Abe, E.; Takakura, H.; Sato, T. J. *Nature* **2000**, *408*, 537.
(15) Wade, K. *Adv. Inorg. Chem. Radiochem.* **1976**, *18*, 1.
(16) Mingos, D. M. P. *J. Chem. Soc, Chem. Commun.* **1983**, 706.
(17) Hume-Rothery, W. *J. Inst. Metals* **1926**, *35*, 295.
(18) Mizutani, U. In *The Science of Complex Alloy Phases*; Massalski, T. B., Turchi, P. E. A., Eds.; TMS (The Minerals, Metals & Materials Society): Warrendale, PA, 2005; pp 1−42.
(19) Tsai, A. P. In *Physical Properties of Quasicrystals*; Stadnik, Z. M., Ed.; Springer: New York, 1999; pp 5−50.
(20) Lin, Q.; Corbett, J. D. *Philos. Mag.* **2006**, *86*, 607.

10.1021/ic700995e CCC: $37.00
Published on Web 09/20/2007

in contrast to other phases in the same ternary system, i.e., the 1/1 AC $Ca_3Au_{12.4}In_{6.1}$ (1.74), the 2/1 AC $Ca_{12.6}Au_{39.0}In_{37.6}$ (2.01), and QC phase $Ca_{14.1}Au_{44.0}In_{41.9}$ (1.98).[21] The new phase is isotypic with binary Zr_7Ni_{10},[22] which stimulates additional interest as to the nature of the electronic transformation (transmutation) process.

Experimental Section

Syntheses. Starting materials were calcium chunks and indium tear drops, both of which were surface-cleaned by a surgical blade before use, and granular gold (all >99.9%, Alfa-Aesar). Appropriate amounts of these were weighed (±0.1 mg) in a N_2-filled glovebox (H_2O < 0.1 ppm vol.) and weld-sealed under an argon atmosphere into tantalum containers, which were in turn enclosed in evacuated SiO_2 jackets to avoid air oxidation of the containers. Samples were heated to 850 °C, held at this temperature for 24 h, and then cooled to 500 °C at a rate of 5 °C/h, followed by annealing there for 2 weeks.

The title phase was first obtained in ~70% yield from the composition $CaAu_{4.5}In_{1.5}$ in a series of reactions designed to tune the hypothetical "$Ca_2Au_6In_5$" to an icosahedral quasicrystal and crystalline approximants.[21] Preliminary single-crystal structural analyses revealed the formula $Ca_4Au_{10}In_3$, and a stoichiometric reaction carried out under the same conditions yielded the pure phase according to its X-ray powder diffraction pattern. This phase is brittle, shiny with a metallic luster, and visually inert to air at room temperature.

SEM-EDX and Magnetism Measurements. Elemental compositions were determined via semiquantitative energy-dispersive X-ray spectroscopy (EDX) on a JEOL 840A scanning electron microscope (SEM) with IXRF X-ray analyzer system and Kevex Quantum light-element detector. To increase the accuracies, samples were mounted in epoxy and carefully polished to avoid possible influences of sample tilting. At least four readings were made on each sample, and the averages were compared with the refined compositions from X-ray diffraction data. Temperature-dependent magnetic susceptibility measurements were performed on a Quantum Design PPMS system in which the magnetic field was controlled at 5 T and temperature was varied from 4 to 300 K.

X-ray Diffraction Analyses. Powder diffraction data were collected on a Huber 670 Guinier powder camera equipped with an area detector and Cu Kα_1 radiation (λ = 1.540598 Å). Finely powdered samples were homogeneously dispersed on a flat Mylar film with the aid of vacuum grease. The detection limit of a second phase with this instrument and system is conservatively estimated to be about 5 vol % in equivalent scattering power, so that an apparently single phase pattern is concluded to represent a >95% phase purity.

Single-crystal data collections were performed with the aid of a Bruker SMART APEX CCD single-crystal diffractometer equipped with graphite-monochromatized Mo Kα (λ = 0.71069 Å) radiation that was operated in an ω scan mode with exposure times of 30 s per frame. Data integration, absorption, and Lorentz polarization corrections were done by the SAINT and SADABS subprograms included in the SMART software packages.[23] Assignment of the space group from the diffractometer data was made on the basis of the Laue symmetry and systematic absence analyses. We noted during the analysis that higher symmetry might be possible judging from the lattice parameters ($b \approx c$) and some possible signatures of pseudo-tetragonal symmetry (a-unique: $x_{Au1} + x_{Au2} \approx 1/2$, $y_{Au1} \approx z_{Au2}$, $z_{Au1} + y_{Au2} \approx 1/2$, $y_{Au3} + z_{Au3} \approx 1/2$, $y_{Ca2} + z_{Ca2} \approx 1/2$, $y_{In2} \approx 1/4$) after a preliminary structure determination. Reflection intensities and symmetries were carefully re-examined with the aid of Platon program,[24] but no higher symmetry or alternative space group was indicated.

Table 1. Some Data Collection and Refinement Parameters for $Ca_4Au_{10}In_3$

space group, Z	*Cmca* (No. 64), 4
fw	2474.5
lattice params	
a (Å)	13.729(4)
b (Å)	10.050(3)
c (Å)	10.160(3)
V (Å^3)	1401.8(6)
d_{calcd} (g/cm^3)	11.73
μ (Mo K$_\alpha$) (mm^{-1})	110.4
extinction coeff.	0.00021(2)
reflns collected	5362 [R_{int} = 0.0641]
obs. data/restraints/params	875/0/46
R1/wR2 [$I > 2\sigma(I)$][a]	0.0349/0.0829
(all data)	0.0389/0.0845
residue peak/hole (e/Å^3)	3.23/−2.70

[a] $R1 = \sum||F_o| - |F_c||/\sum|F_o|$; $wR2 = \{[\sum[w(F_o^2 - F_c^2)^2]/\sum[w(F_o^2)^2]\}^{1/2}$.

Structure refinements of two data sets (from crystals from different reactions, one synthesized with a deficiency of Ca) were performed with the aid of the SHELXTL subprogram,[23] and both yielded substantially the same results with no evidence of any homogeneity range in this direction. Therefore, those for the crystal from the stoichiometric reaction are reported here. Direct methods yielded seven peaks, of which three were assigned to Au, two to In, and two to Ca atoms according to the peak heights and separations. Subsequent least-square refinements proceeded smoothly and converged at R1 ≈ 6.1%. No Au/In admixtures were suggested according to rather uniform isotropic displacement parameters (U_{eq} = 0.0077−0.011 Å^2). The least certain case on refinement was for the In2 position, for which In/Au was 97/3(1)%. Accordingly, all occupancy parameters were constrained to 100%. The final anisotropic refinement, with a secondary extinction correction, converged at R1 = 3.49%, wR2 = 8.29% for 46 variables and 875 independent reflections. The refined composition is $Ca_4Au_{10}In_3$, consistent with the EDX result, $Ca_{3.7(2)}Au_{10}In_{2.9(1)}$.

A summary of crystal and structural refinement data is in given in Table 1, and the refined positional parameters standardized with TIDY[25] are listed in Table 2 together with isotropic-equivalent displacement parameters. The nearest-neighbor interatomic distances are listed in Table 3. The remaining data are deposited in the Supporting Information (Table S1, cif).

Electronic Structure Calculations. These were performed by the self-consistent, tight-binding, linear-muffin-tin-orbital (LMTO) method in the local density and atomic sphere approximations (ASA), within the framework of the DFT method.[26−29] The ASA radii were calculated automatically with a maximum overlap restriction of 18%. There was no need for any empty sphere, and

(21) Lin, Q.; Corbett, J. D. *J. Am. Chem. Soc.* **2007**, *129*, 6789.
(22) Joubert, J.-M.; Černý, R.; Yvon, K.; Latroche, M.; Percheron-Guégan, A. *Acta Crystallogr.* **1997**, *C53*, 1536.
(23) *SHELXTL*; Bruker AXS, Inc.; Madison, WI, 1997.
(24) Spek, A. L. *J. Appl. Crystallogr.* **2003**, *36*, 7.
(25) Gelato, L. M.; Parthé, E. *J. Appl. Crystallogr.* **1987**, *20*, 139.
(26) Jepsen, O.; Snob, M. *Linearized Band Structure Methods in Electronic Band-Structure and its Applications, Springer Lecture Note*; Springer-Verlag: Berlin, 1987.
(27) Shriver, H. L. *The LMTO Method*; Springer-Verlag: Berlin, 1984.
(28) Tank, R.; Jepsen, O.; Burkhardt, A.; Andersen, O. K. *TB-LMTO-ASA Program, Vers. 4.7*; Max-Planck-Institut für Festkörperforschung; Stuttgart, Germany, 1994.
(29) Anderson, O. K.; Jepsen, O. *Phys. Rev. Lett.* **1984**, *53*, 2571.

Table 2. Atomic Coordinates and Isotropic-Equivalent Displacement Parameters for $Ca_4Au_{10}In_3$

atom[b]	Wyckoff	symmetry	*x*	*y*	*z*	U_{eq} (Å^2)
Ca1	8*d*	2.	0.3021(3)	0	0	0.0054(8)
Ca2	8*f*	m.	0	0.3030(4)	0.2020(4)	0.0070(9)
Au1	16*g*	1	0.14132(4)	0.02778(6)	0.20681(6)	0.0076(2)
Au2	16*g*	1	0.35878(4)	0.29340(5)	0.01841(6)	0.0085(2)
Au3	8*f*	*m.*	0	0.09760(8)	0.40455(8)	0.0073(2)
In1	4*a*	2/*m.*	0	0	0	0.0087(5)
In2	8*e*	.2.	1/4	0.2685(1)	1/4	0.0067(3)

[a] U_{eq} is defined as one-third of the trace of the orthogonalized U_{ij} tensor. [b] The Ca and In atom sites as listed parallel the positions occupied by Zr3, Zr1 and Zr4, Zr2, respectively, in Zr_7Ni_{10}.

Table 3. Interatomic Distances (Å) in the Structure of $Ca_4Au_{10}In_3$[a]

Ca1−Au1 × 2	3.060(3)	Ca2−Au1 × 2	3.119(3)	In1−Au1 × 3	2.8736(8)
Au1 × 2	3.091(1)	Au2 × 2	3.116(3)	Au2 × 4	2.8469(8)
Au2 × 2	3.055(1)	Au3	2.915(4)	Ca2 × 2	3.618(4)
Au2 × 2	3.037(3)	Au3	3.153(4)	Ca2 × 2	3.672(4)
Au3 × 2	3.047(4)	Au3	3.183(5)	In2−Au1	2.876(1)
In2 × 2	3.518(1)	Au1 × 2	3.379(3)	Au1 × 2	3.034(2)
In2 × 2	3.774(1)	Au2 × 2	3.441(4)	Au2	2.7981(8)
Ca2 × 2	3.939(4)	In1	3.618(4)	Au2 × 2	3.1709(9)
		In1	3.672(4)	Ca1 × 2	3.518(1)
		In2 × 2	3.484(1)	Ca2 × 2	3.484(1)
Au1−Au1	3.110(1)	Au2−Au1	2.910(1)	Au3−Au1 × 2	2.880(1)
Au2	2.910(1)	Au1	3.035(1)	Au2 × 2	2.8712(9)
Au2	3.035(1)	Au2	3.134(1)	Au3	2.759(2)
Au3	2.880(1)	Au3	2.8712(9)	Ca1 × 2	3.047(4)
In1	2.8736(8)	In1	2.8469(8)	Ca2	2.915(4)
In2	2.876(1)	In2	2.7981(8)	Ca2	3.153(4)
In2	3.034(2)	In2	3.1709(9)	Ca2	3.183(5)
Ca1	3.060(3)	Ca1	3.037(3)		
Ca1	3.091(1)	Ca1	3.055(1)		
Ca2	3.119(3)	Ca2	3.116(3)		
Ca2	3.379(3)	Ca2	3.441(4)		

[a] All distances within the first coordination sphere are listed.

all calculated WS (Wigner−Seitz) radii were reasonable: 3.40−3.64 Å for Ca, 3.04−3.13 Å for Au, and 3.16−3.23 Å for In. Reciprocal space integrations were carried out using the tetrahedron method. Down-folding techniques were automatically applied to the LMTOs, and scalar relativistic effects were included in the calculations. The band structure was sampled at 24 × 24 × 24 *k* points in the irreducible wedge of the first Brillouin zone.

Mulliken population analyses of $Ca_4Au_{10}In_3$ and Zr_7Ni_{10} were also performed with the aid of CAESAR,[30] a semiempirical EHTB band calculation program, in order to estimate relative site potentials, particularly regarding any differentiation among the Zr sites with respect to Ca versus In substitution therein. The following orbital energies and exponents from the literature were employed in the initial set of calculations: (H_{ii} = orbital energy (eV), ξ = Slater exponent): Ca: 4s, $H_{ii} = -5.342$, $\xi = 1.069$; 4p, $H_{ii} = -3.569$, $\xi = 0.893$; Au: 6s, $H_{ii} = -10.92$, $\xi = 2.602$; 6p, $H_{ii} = -5.55$, $\xi = 2.584$; 5d, $H_{ii} = -15.076$, $\xi_{11} = 6.163$, $c1 = 0.6851$; $\xi_{22} = 2.794$, $c2 = 0.5696$; In: 5s, $H_{ii} = -12.6$, $\xi = 1.903$; 5p, $H_{ii} = -6.19$, $\xi = 1.677$;[31] Zr: 5s, $H_{ii} = -8.00$, $\xi = 1.817$; 5p, $H_{ii} = -5.40$, $\xi = 1.776$; 4d, $H_{ii} = -10.20$, $\xi_{11} = 3.835$, $c1 = 0.6210$, $\xi_{22} = 1.505$, $c2 = 0.5769$;[32] Ni: 4s, $H_{ii} = -9.17$, $\xi = 1.825$; 4p, $H_{ii} = -5.15$, $\xi = 1.125$; 3d, $H_{ii} = -13.49$, $\xi_{11} = 5.75$, $c1 = 0.5683$; $\xi_{22} = 2.00$, $c2 = 0.6292$.[33]

The above Ni 3d energy appears more suitable for cationic states, so the H_{ii} data first for Ni and then for both Ni and Zr were charge-iterated to self-consistency. These caused the relative Zr site charges to become negative, and those for Ni, positive, but the differentiation among the former remained consistent as to both order and relative charges. Therefore, the first set of results is quoted later. The substitution of Au for Ni has a major effect on the bonding and charge distributions.

Results and Discussion

The title compound is the first ternary derivative of the Zr_7Ni_{10} type.[22] Notably, no other binary compounds have been structurally analyzed in this family, although Zr_7Cu_{10}, Hf_7Ni_{10}, and Hf_7Cu_{10} have been so assigned according to powder data.[34,35] The fact that $Ca_4Au_{10}In_3$ and Zr_7Ni_{10} are isotypic is very surprising because electropositive Ca and electronegative In in $Ca_4Au_{10}In_3$ are ordered among the same Wyckoff positions as is electropositive Zr in Zr_7Ni_{10}.

Crystal Structures. For convenience, we first present a structural comparison between the isotypic Zr_7Ni_{10} and $Ca_4Au_{10}In_3$, Pearson symbol oC68. The parent Zr_7Ni_{10},[22] Figure 1, features a 3D nickel framework consisting of remarkable sinusoidal layers (d_{Ni-Ni} = 2.624−2.726 Å). Such layers are stacked along the *b* axis with only slightly longer Ni1−Ni2 (2.732 Å) and Ni3−Ni3 (2.776 Å) interlayer bonds. For clarity, the latter are de-emphasized by means of light gray "bonds" in Figure 1. The Zr atoms, color-coded according to their equivalencies in $Ca_4Au_{10}In_3$, are sandwiched between neighboring layers. Naturally, $Ca_4Au_{10}In_3$ inherits the sinusoidal layered feature, but it exhibits a more complex 3D polyanion framework, as shown in Figure 2a, owing to distinctly stronger Au−Au and Au−In interlayer interactions, as revealed by the Mulliken overlap population analyses (below). Note that the sinusoidal character of the layers in the Au substructure are less pronounced compared with the Ni framework in Zr_7Ni_{10}; the interlayer bonds, Au1−Au2 [3.035(1) Å] and Au3−Au3 [2.759(2) Å], are comparable to, even a bit shorter than, the intralayer Au−Au bonds [2.8712(9)−3.134(1) Å]. A more informative view of the $[Au_{10}In_3]$ polyanionic network is found projected along the $\sim[0\bar{1}1]$ direction in Figure 2b, rather than along alternative axial directions. As can be seen, the Au layer contains numerous distorted pentagonal and hexagonal rings, typical for Au polyanions.[36]

(30) Ren, J.; Liang, W.; Whangbo, M.-H. *CAESAR for Windows*; Prime-Color Software, Inc., North Carolina State University: Raleigh, NC: 1998.
(31) Hoffmann, R.-D.; Pöttgen, R.; Landrum, G. A.; Dronskowski, R.; Künnen, B.; Kotzyba, G. *Z. Anorg. Allg. Chem.* **1999**, *625*, 789.
(32) Canadell, E.; Mathey, Y.; Whangbo, M.-H. *J. Am. Chem. Soc.* **1988**, *110*, 104.
(33) Alvarez, S. *Table of Parameters for Extended Hückel Calculations, Part 1*; Univesitat de Barcelona: Barcelona, Spain, 1987.
(34) Besenko, L. *Acta Crystallogr.* **1975**, *40*, 365.
(35) Kirkpatrick, M. E.; Smith, J. F.; Larsen, W. L. *Acta Crystallogr.* **1962**, *15*, 894.
(36) Dai, J.; Corbett, J. D. *Inorg. Chem.* **2007**, *46*, 4592.

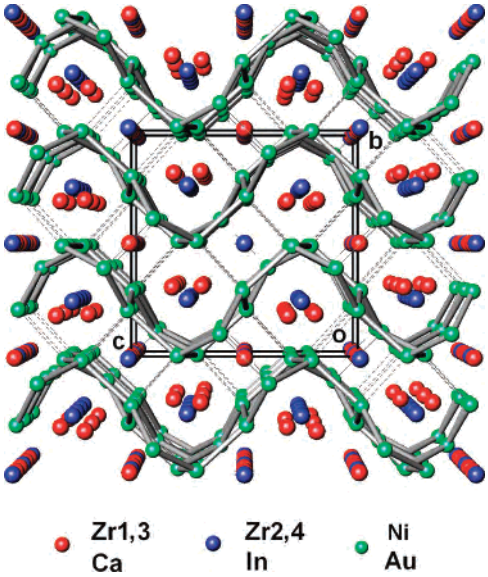

Figure 1. Perspective view of Zr_7Ni_{10} along the [100] direction, in which the remarkable sinusoidal layers of Ni are highlighted. The slightly longer interlayer Ni−Ni bonds are deemphasized for clarity. The Zr1, Zr3 and Zr2, Zr4 type sites are represented by red and blue spheres, respectively, for comparisons with Ca and In placements in isotypic $Ca_4Au_{10}In_3$.

The environments of the four independent Zr atoms in Zr_7Ni_{10}[22] are quite different, namely, each Zr1 is surrounded by 11 Ni atoms, Zr3, by 10, and Zr2 and Zr4, each by eight, meaning that Zr1 and Zr3 are located in the larger cavities. Dimensionally, this could account for Ca atoms in the ternary occupying the Zr1 and Zr3 sites, whereas the In atoms go onto the Zr2 and Zr4 sites, consistent with relative Ca and In metallic radii (CN = 12: Ca, 1.970; In, 1.579 Å).[37] Panels a and b of Figure 3 show the nearest-neighbor environments of Ca1 and Ca2, respectively. The former is surrounded by 10 Au and four In atoms that define a polyhedron with a vertical 2-fold rotational axis along *a* that bisects the Au3−Au3 bond, whereas Ca2 is bounded by (7 + 4) Au and four In in a polyhedron with a vertical mirror plane perpendicular to the *a* axis that also contains the Au3−Au3 bond. The Ca−Au distances about Ca2 are appreciably longer (see Table 3) than about Ca1, but both groups of distances are distinctly shorter (by ∼0.4 Å) than Ca−In distances. Note that both polyhedra in Figure 3 exhibit pairs of equivalent and substantially planar Au3−Au3−Au2−Au1−In2 pentagonal faces (bold blue bonds) that are nearly perpendicular (±2.8°) to each other. Each Ca1@$Au_{10}In_4$ polyhedron shares these pentagonal faces with two neighboring Ca2@$Au_{10}In_5$ polyhedra, and vice versa. The result is a $Ca_4Au_{28}In_{12}$ tetramer unit (Figure 3c) of two Ca1 and two Ca2 clusters that share a common Au3−Au3 edge (d = 2.759 Å), the shortest Au−Au bond in the structure. The structure therefore may be alternatively viewed as a condensed solid of $Ca_4Au_{28}In_{12}$ units (Figure S1). In addition, the closest Ca1 and Ca2 separations are 3.939 Å, twice Pauling's metallic radii for CN = 12, 3.94 Å.[37] According to the COHP data (below), however, these Ca−Ca pairs are poorly bonded, suggesting that their separation in essence arises from just a matrix effect imposed by the shared polyanions. Actually, short Ca−Ca separations are very common for intermetallics containing Au polyanionic frameworks, e.g., in CaAuIn (3.85−3.89 Å), CaAuGe (3.62−3.90 Å), CaAuSn (3.71−3.79 Å),[38] and $Ca_3Au_{6.61}Ga_{4.39}$ (3.75 Å).[39]

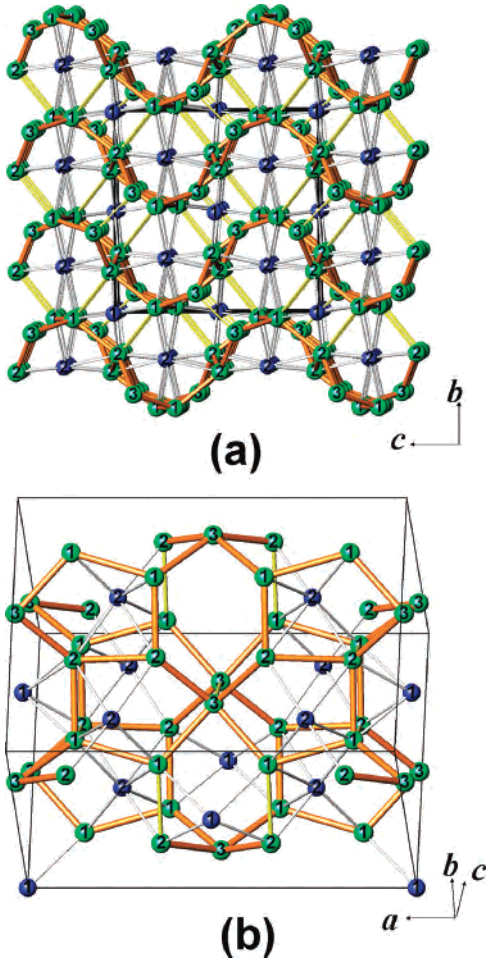

Figure 2. Polyanion framework of $Ca_4Au_{10}In_3$ projected along (a) [100] and (b) ∼[0$\bar{1}$1] directions, with Ca atoms (red spheres in Figure 1) omitted for clarity. The intralayer Au−Au bonds are shown as bold golden lines, whereas the interlayer Au−Au and Au−In bonds are represented as thin yellow and gray lines, respectively, even though they are comparable in length. Green spheres represent Au, and blue, In.

Electronic Structure and Chemical Bonding. Figure 4a shows the densities-of-states (DOS) of $Ca_4Au_{10}In_3$ calculated by TB−LMTO−ASA methods. The Fermi level E_F (dashed line) lies in a continuous DOS region, indicating a metallic character for the compound. The latter is consistent with the measured Pauli-like paramagnetic property ($\chi \approx 4.77 \times 10^{-5}$ emu/g, Figure S2), reflecting delocalized unpaired electrons in a metallic material. The crystal orbital Hamilton population (−COHP) data for each of the bond types as a function of energy, Figure 4b, show some remarkable bonding properties; all interactions remain bonding up to nearly 1.5 eV, at which point the dominant Au−In data turn antibonding in character. The calculated integrated −COHP data (−ICOHP, eV/bond) up

(37) Pauling, L. *The Nature of the Chemical Bond*, 3rd ed.; Cornell University Press: Ithaca, NY, 1960; pp 393−448.

(38) Kuβmann, D.; Hoffmann, R.-D.; Pöttgen, R. *Z. Anorg. Allg. Chem.* **1998**, *624*, 1727.

(39) Kussmann, D.; Hoffmann, R.-D.; Pöttgen, R. *Z. Anorg. Allg. Chem.* **2000**, *627*, 2053.

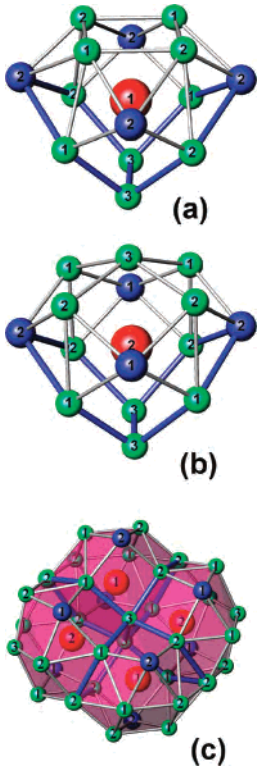

Figure 3. Polyhedral views of (a) Ca1, (b) Ca2 (red), and (c) the tetrameric $Ca_4Au_{28}In_{12}$ units in the structure of $Ca_4Au_{10}In_3$. The pentagonal faces in all are highlighted with bold blue bonds. Red spheres represent Ca, green, Au, and blue, In. (The condensation of $Ca_4Au_{28}In_{12}$ tetrameric units is shown in Figure S1.)

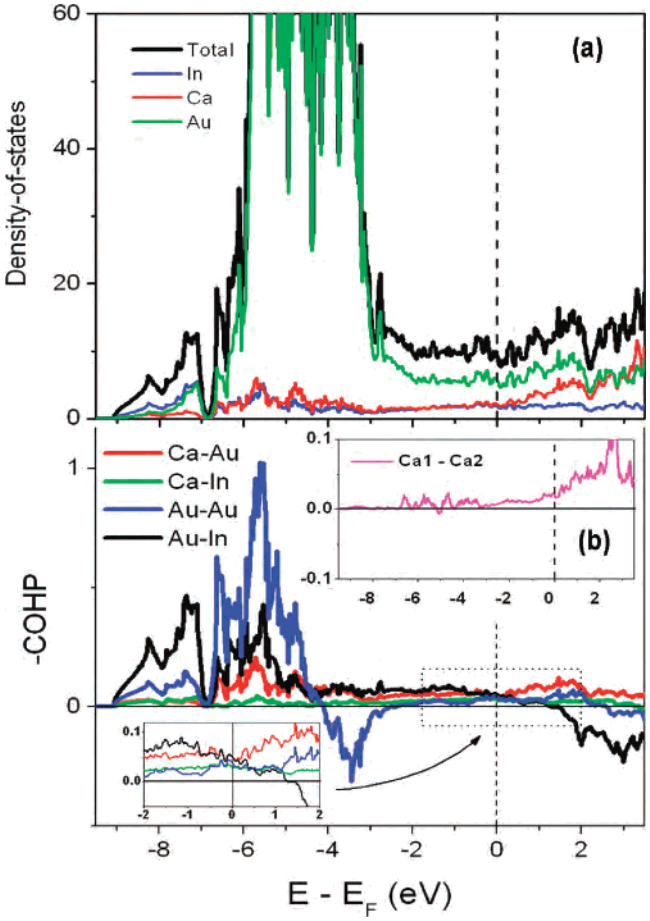

Figure 4. (a) Densities-of-states (DOS) and (b) crystal orbital Hamilton populations (−COHP) per bond for $Ca_4Au_{10}In_3$ from LMTO calculations. Insets: −COHP data for Ca1−Ca2 and an enlarged portion of −COHP data as marked.

to E_F for each bond type are 1.10 for Au−Au, 1.18 for Au−In, 0.50 for Ca−Au, 0.18 for Ca−In, and 0.07 for Ca−Ca. These values indicate dominant Au−Au and Au−In bonding interactions in this phase, consistent with EHTB analyses (below). Surprisingly, the DOS show a rather distinct but shallow dip (or pseudogap) at e/a = 2.35, above E_F, suggesting the presence of some special electronic state that may be chemically tunable under rigid band assumptions.[6,21] But this calculation *fails* predict the known QC (e/a = 1.98)!

In comparison, Zr_7Ni_{10} (e/a = 1.65 without Ni d^{10}) also shows empty bonding states and a remarkably deep pseudogap (e/a = 2.79) well above E_F according to LMTO analyses (Figure S3). Since three phases with somewhat higher e/a values, i.e., the 1/1 AC $Ca_3Au_{12.4}In_{6.1}$(1.74), the 2/1 AC $Ca_{12.6}Au_{39.0}In_{37.6}$ (2.01), and the QC $Ca_{14.1}Au_{44.0}In_{41.9}$ (1.98) have already been found[21] not far from $Ca_4Au_{10}In_3$ (e/a = 1.59), whether Zr_7Ni_{10} might be a precursor for tuning to special electronic states, quasicrystalline or not, is under further investigation.

Electronic disparities in Zr_7Ni_{10} structure types. As mentioned, the Zr2 and Zr4 sites in the binary Zr_7Ni_{10} are subsequently occupied by In atoms, and Zr1 and Zr3, by Ca, in the polarized ternary derivative $Ca_4Au_{10}In_3$. Therefore, Mulliken population analyses were performed for both structures in order to evaluate the electronic disparities, or atom coloring options, in these two cases.

Table 4 lists the nominal atomic site charges, that is, Mulliken populations relative to atomic valence electron counts (VEC),[4] as well as Mulliken bond overlap populations for both $Ca_4Au_{10}In_3$ and Zr_7Ni_{10}. The calculated site charges for all Zr sites in the latter are far less positive than what might be expected for Zr acting as a cation, suggesting significant covalent bonding with Ni, which behavior is also consistent with the significantly short Zr−Ni interatomic distances (2.60−2.75 Å).[22] Actually, the Zr site charges divide into two subgroups: (1) Zr1 and Zr3, with somewhat higher charge values (0.22 and 0.44); and (2) Zr2 and Zr4, with lower charge values (0.14 and 0.19), following the

Table 4. Net Charges Per Atom (q) and Mulliken Overlap Populations Per Bond (OP) for $Ca_4Au_{10}In_3$ and Zr_7Ni_{10} Calculated by the EHTB Method[a]

$Ca_4Au_{10}In_3$		Zr_7Ni_{10}	
q(Ca1)	+1.49	q(Zr3)	+0.44
q(Ca2)	+1.43	q(Zr1)	+0.22
q(In1)	−0.18	q(Zr4)	+0.19
q(In2)	−0.34	q(Zr2)	+0.14
q(Au1)	−0.46	q(Ni1)	−0.16
q(Au2)	−0.47	q(Ni2)	−0.16
q(Au3)	−0.62	q(Ni3)	−0.26
OP (Ca−Ca)	0.02	OP (Zr1−Zr3)	0.13
OP (Ca−Au)	0.09	OP [Zr(1,3)−Ni)]	0.17
OP (Ca−In)	0.07	OP [Zr(1,3)−Zr(2,4)]	0.18
OP (Au−Au)	0.20	OP [(Ni−Ni)]	0.07
OP (Au−In)	0.36	OP [Zr(2,4)−Ni]	0.23

[a] For comparison, atoms on same Wyckoff positions and the corresponding OPs are listed on the same lines.

coordination number differences mentioned above. These do not differentiate further with the use of empirical, charge-consistent energy parameters for Zr and Ni, and their charge types unreasonably invert (see Experimental Section). Considering the so-called electronic disproportionation that accompanies the interconversion between the two compounds, the latter two sites are obviously more suitable for topologic substitution by the more electronegative In atoms according to their differentiation in $Ca_4Au_{10}In_3$ (left block, Table 4). Although the site population difference between the Zr1 (0.22) vs Zr4 (0.19) sites is not large, the distances and atom environments about these two become strongly differentiated after the parallel substitution of Ca and In. The alternative exchange of Ca2 and In1 at this stage would have clear disadvantages, not only in bonding interactions (below) but also in size. The present In1 (vice Zr4) cavity is distinctly smaller, with only seven interactions with Au around 2.86 Å (Table 3); if a switch to the present Ca2 position (Zr1) were to occur, seven long In−Au interactions averaging 3.10 Å plus four more around 3.4 Å would result. Four In−In separations would also be generated around 3.56 Å, too long to be significant. Simultaneously, the present In1 site radius is around 0.3 Å less, too small for Ca2. Although some distortions might accommodate the distance problems around the switched atoms, the ternary structure may be too tight and complex to allow this much change.

In terms of the bonding interactions, some remarkable differences between $Ca_4Au_{10}In_3$ and Zr_7Ni_{10} are found in the relative overlap population per bond (OP), Table 4. Those for Zr−Zr and Zr−Ni pairs in Zr_7Ni_{10} are much larger than that for the Ni−Ni pair (a reasonable result for a late 3d element in the presence of electron-donating Zr), whereas in $Ca_4Au_{10}In_3$, the Au−Au and Au−In OPs become substantial. These facts reveal that layer OPs mainly migrate from Zr−Zr and Zr−Ni to Au−Au and Au−In, conveying some complicated chemical alterations between the Zr_7Ni_{10} and $Ca_4Au_{10}In_3$ isotypes. The −COHP data for the two cases reveal similar figurative migration of OPs. The Zr−Ni and Zr−Zr results (Figure S3) remain substantial at and beyond E_F, whereas Ni−Ni becomes and stays antibonding below E_F, suggesting a filled d band. As a comparison, the Au−Au and Au−In −COHP values are dominant at and beyond E_F (although a filled d band for Au is still suggested), whereas Ca−Au and Ca−In data show appreciable positive −COHP values above E_F.

Acknowledgment. We thank Kevin W. Dennis for collection of the magnetic data and one reviewer for pointing out the implied problems with the initial EHTB energies. This research was supported by the U.S. National Science Foundation, Solid-State Chemistry, via Grant No. DMR-0444657 and was performed in the facilities of the Ames Laboratory, U.S. Department of Energy.

Supporting Information Available: Figures S1−S3, Table S1, and CIF data. This material is available free of charge via the Internet at http://pubs.acs.org.

IC700995E